ORIGINAL ARTICLE

A Suite of Modular Fluorescence Assays Interrogate the Human Immunodeficiency Virus Glycoprotein-41 Coiled Coil and Assist in Determining Binding Mechanism of Low Molecular Weight Fusion Inhibitors

AU1 *Miriam Gochin*[1,2]

[1]*Department of Basic Science, Touro University-California, Vallejo, California.*
[2]*Department of Pharmaceutical Chemistry, University of California, San Francisco, California.*

ABSTRACT

Several different segments of the gp41 N-heptad repeat coiled coil have been constructed using N-terminal bipyridyl modification of composite peptides and inducing trimerization by adding ferrous ions. These metallopeptides act as receptors in fluorescence-binding assays with apposing fluorescently labeled C-peptide probes. The Fe^{II} coordination complex quenches C-peptide fluorescence upon binding, and reversal of quenching by a small molecule inhibitor can be used to obtain the inhibitor-binding constant. A total of 10 peptide pairs targeting 25–46 residue segments of the coiled coil were constructed, with C-peptide probes of different lengths and binding affinities. The result is a suite of assays for exploring binding in the mM to nM range to any desired region of the coiled coil, including the hydrophobic pocket (HP), extended regions on either side of the pocket, or a region associated with T20 resistance mutations. These assays are high-throughput ready, and could be used to discover novel compounds binding along various regions of the gp41 coiled coil groove. They were used to evaluate a sub-μM low molecular weight fusion inhibitor, resulting in the finding that the molecule bound specifically to the HP and attained its potency from a low off-rate.

INTRODUCTION

Entry inhibitors are a relatively new class of approved human immunodeficiency virus type 1 (HIV-1) drugs, and have promising properties for combating resistance to current treatments and for prophylaxis.[1,2] They can act in both immune cell protection and disease prevention by targeting the steps of the viral life cycle that occur before infection of host cells. Fusion inhibitors are a class of entry inhibitors that act on the HIV transmembrane protein gp41, which is universally required by all strains for initial infection or cell-to-cell transmission.[3–5] A large conformational change occurs in gp41 during fusion, involving exposure of a homotrimeric N-heptad repeat (NHR) coiled coil and subsequent folding of antiparallel C-heptad repeat (CHR) helices down the grooves of the coiled coil, to form a trimer of hairpins, a prerequisite for effective fusion pore formation.[2]

The gp41 coiled coil has been considered an important target for fusion inhibitors, based on peptides studies, which show that CHR peptides are highly effective fusion inhibitors.[6–8] These include T20, currently the only FDA-approved fusion inhibitor.[9] Small AU2 molecule fusion inhibitors have been sought for many years, but with limited success, having only μM potency against fusion.[10,11] They have chiefly targeted a known hydrophobic pocket (HP) on the coiled coil. However, in many cases, there is little experimental evidence confirming the exact binding site and no way to test inhibitors against different sites along the coil. Finding two inhibitors that bind in adjacent sites could enable a fragment-based drug design approach, in which a linker connecting two adjacent-binding fragments can have a multiplicative effect on their binding affinity.[12]

In previous work, we have demonstrated the use of metal–bipyridyl coordination to stabilize a segment of the gp41 coiled coil representing the HP,[13] as well as an extended receptor targeting adjacent sites and high-affinity interactions.[14,15] This study expands on the analysis of inhibitors detected with these assays, and introduces a new assay that focuses on the N-terminal end of the coiled coil, a site prone to development of resistance mutations in viruses exposed to T20.[16] C-peptide probes have been designed for fluorescence intensity assays that interrogate the NHR subsections. Adjusting C-peptide length tuned both assay selectivity and the range of detectable affinities. Small molecule inhibitors could easily be detected by competitive inhibition, as we have shown previously.

ABBREVIATIONS: 6HB, six helix bundle; CHR, C-heptad repeat; FL, fluorescein; Gp41, glycoprotein-41; HIV-1, human immunodeficiency virus type 1; HP, hydrophobic pocket; LY, lucifer yellow; NHR, N-heptad repeat.

DOI: 10.1089/adt.2012.464

Comparison of the results with the known biological activity of peptide segments of the CHR[17] and small molecules[18] confirmed the relevance of these biochemical screening assays for detection of fusion inhibitors. The ease and rapidity of the assays lends them to implementation in a high volume format. Utilization of the assays could result in identification of novel fragments or small molecules binding at specific subsites, with the possibility of linking them to generate high-affinity nonpeptide inhibitors. This concept has been applied for the derivation of C-peptide inhibitors of HIV-1 fusion containing multifunctional domains.[2,17]

MATERIALS AND METHODS

Materials

Peptides were prepared by solid-phase synthesis (Biosynthesis, Inc.). Small molecules were prepared according to previously published procedures.[18] Fluorescein (FL) and Lucifer yellow (LY) were purchased from Molecular Probes (Invitrogen) as iodoacetamides and covalently attached through standard cysteine disulfide chemistry according to the manufacturer's instructions. AU2 Labeled peptides were purified by HPLC using acetonitrile: H_2O AU2 with 0.05% TFA.

Circular Dichroism Experiments

Circular dichroism (CD) studies were performed on a DSM20 CD spectrophotometer from On-Line Instruments Systems, Inc., using 20 μM solutions of peptides in a 15 mM Tris-acetate buffer, pH 7.0, at 25°C.

Fluorescence Intensity Measurements

Fluorescence intensity was measured in 384-well low-volume plates (Greiner Bio-one) on a Spectramax M5 plate reader (Molecular Devices). Env# concentration was determined in 6 M Gdn.HCl from the absorbance at 291 nm, using the extinction coefficients of bipyridine ($\varepsilon_{291} = 12{,}000$) plus the calculated contribution of any Trp and Tyr residues in the peptide sequence (www.expasy.org). FL-labeled peptide concentration was determined using $\varepsilon_{495} = 93{,}000\ M^{-1}\ cm^{-1}$ in 6 M Gdn.HCl at pH 9; LY-labeled peptide concentration was determined using $\varepsilon_{425} = 10{,}800\ M^{-1}\ cm^{-1}$ in 6 M Gdn.HCl. Fe(env#)$_3$ complexes were prepared by the addition of 1/3 stoichiometry of a freshly prepared ferrous solution to peptides in a 25 mM Tris-acetate buffer, pH 7.0. Fluorescence assays were carried out using a constant concentration of probe peptide, typically 15 nM of FL-labeled peptide or 200 nM of LY-labeled peptide. Typical receptor concentrations used in inhibition experiments were 3.6 μM [Fe(env2.0)$_3$/C18-e2.0FL] 75 nM [Fe(env5.0)$_3$/C32-e5.0FL], 1.5 μM [Fe(env5.0)$_3$/C28-e5.1FL/LY], 3 μM [Fe(env5.0)$_3$/C21-e6.0FL/LY], 3 μM [Fe(env6.0)$_3$ or Fe(env5.1)$_3$/C28-e5.1LY/C21-e6.0LY], and 0.75 μM Fe(env6.0)$_3$/C21-e6.0FL. Receptor concentrations are always reported as concentration of monomer env# peptide, which should be equal to the concentration of binding sites on three equivalent faces of the coiled coil. Fractional fluorescence values are reported relative to a control in which the Fe(env#)$_3$ receptor was omitted. The detailed T1 T2 protocol is provided in *Tables 1* and *2*.

Table 1. Assay Protocol Table (C18-e2.0LY/FL, C21-e6.0LY)

Step	Parameter	Value	Description
1	Control in odd wells	9.6 μL	1:1 P = 2X Cn-e#Fl/LY and B = buffer
2	Assay in even wells	9.6 μL	1:1 P and R = 2X Fe(env#)$_3$
3	Assay readout	Ex 485 (FL) or Ex 425 (LY) Em 538	Fluorescence intensity plate reader
4	Library compounds	0.4 μL	In DMSO, all wells
5	Incubation time	0–30 min	Sample equilibration
6	Assay readout	Ex 485 (FL) or Ex 425 (LY) Em 538	Fluorescence intensity plate reader

Step Notes

1. Greiner low volume tapered black/clear 384-well plates; P = 30 nM Cn-#FL or 400 nM Cn-#LY in 0.02% Tween-20, 25 mM Tris, 25 mM acetic acid, pH 7.0, B = buffer (no Tween).
2. R = 7.2 μM Fe(env2.0)$_3$ or 6 μM Fe(env5.0)$_3$ or 6 μM Fe(env6.0)$_3$ with C21-e6.0LY in a buffer (concentration of monomer peptide).
3. Determine assay bounds F_{max}, F_{min} and Z′.
4. To determine K_i, use serial dilution.
5. Measure immediately and at 15 min intervals for up to 1 h, to allow for equilibration.
6. Fractional fluorescence = $(F_s \pm \sigma_s)/\langle F_c \rangle$, where $\langle F_c \rangle$ is the average value of the control fluorescence in odd wells, and F_s is the fluorescence of the sample. Large increase in control values with compound concentration indicates compound interacts with probe, for example, by micelle formation.

DMSO, dimethyl sulfoxide; LY, lucifer yellow; FL, fluorescein.

RESULTS AND DISCUSSION

Peptide Design

The array of overlapping segments used to scan the full-length coiled coil is shown in *Figure 1*. NHR peptide env2.0 contained the F1 residues $_{565}$LLQLTVWGIKQLQARIL$_{581}$ of the HP, as previously described,[13] and env3.0[14] and env4.0 were extended to include a region either C-terminal or N-terminal to the pocket, respectively. Env5.0 and env5.1 extended the N-terminal region even further,[15] and env6.0 contained just the N-terminal end of the coiled coil, without the HP. This region binds to the N-terminal two-thirds of T20. The env# peptides were modified with an N-terminal 5-carboxybipyridine (bpy) group and a linker sequence GQAV. Three bidentate bpy groups formed an octahedral complex with transition metal ions, stabilizing the trimeric form of the env# receptors.

Figure 1 also depicts CHR peptides that were synthesized, aligned antiparallel to the NHR peptides, and labeled according to the number of residues and the cognate receptor. C18-e2.0 covered the HP and N-terminal adjacent region. C28-e5.1 and C21-e6.0 mimicked portions of T20 and did not contain HP-binding residues. C32-e5.0 and C39-e5.1 spanned close to the full length CHR. A fluorescent marker, LY or FL, was attached to each CHR peptide probe through a C-terminal cysteine, so that NHR–CHR binding could be followed by fluorescence

Table 2. Assay Protocol Table (C32-e5.0FL, C28-e5.1LY/FL, C21-e6.0FL)

Step	Parameter	Value	Description
1	Probe P in all wells	4.8 μL	P = 2X Cn-e#Fl/LY
2	Library compounds	0.4 μL	In DMSO, all wells
3	Buffer B in odd wells	4.8 μL	Buffer B
4	Receptor R in even wells	4.8 μL	R = 2X Fe(env#)$_3$
5	Incubation time	0–30 min	Sample equilibration
6	Assay readout	Ex 485 (FL) or Ex 425 (LY) Em 538	Fluorescence intensity plate reader

Step Notes

1. Greiner low volume tapered black/clear 384-well plates; P = 30 nM Cn-#FL or 400 nM Cn-#LY in 0.02% Tween-20 in a buffer.
2. To determine K_i, use serial dilution.
3. B = 25 mM Tris, 25 mM acetic acid, pH 7.0.
4. R = 150 nM Fe(env5.0)$_3$ with C32-e5.0FL, 3 μM Fe(env5.0)$_3$ with C28-e5.1FL/LY, 2 μM Fe(env6.0)$_3$ with C28-e5.1FL/LY, 1.5 μM Fe(env6.0)$_3$ with C21-e6.0FL in a buffer (concentration of monomer peptide).
5. Measure immediately and at 15 min intervals for up to 1 h, to allow for equilibrium.
6. Fractional fluorescence = $(F_s \pm \sigma_s)/\langle F_c \rangle$, where $\langle F_c \rangle$ is the average value of the control fluorescence in odd wells, and F_s is the fluorescence of the sample. Large increase in control values with compound concentration indicates compound interacts with a probe, for example, by micelle formation.

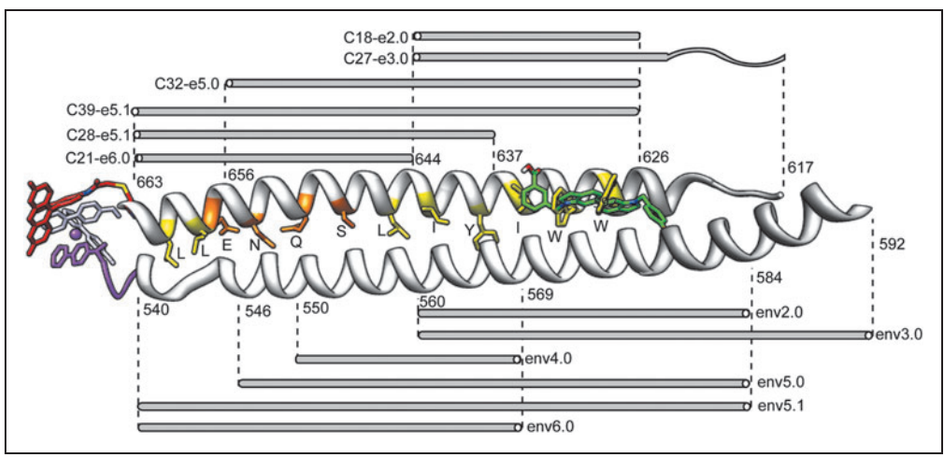

Fig. 1. Helical NHR and CHR domains of the gp41 extracellular region, showing the location of env# constructs and assay C-peptide probes listed in Table 3. For simplicity, only one NHR and CHR helix is shown from the trimer. The model shown is from PDB structures 2X7R[22] (light gray) and 1IF3[39] (gray). Residues at *i*, *i*+4, *i*+7 positions of the CHR are indicated in yellow (hydrophobic) or orange (polar). Env# peptides are bipyridylated and studied complexed to 1/3 stoichiometry Fe(II) (shown in purple and light purple for env6.0). C-peptides are labeled with a fluorophore at a C-terminal cysteine (fluorescein shown for C21-e6.0 in red). Env peptides contain the wild-type sequence, while C-peptides are mutated to increase helicity and affinity (see text). A known hydrophobic pocket binding small molecule 14g is shown in green (binding pose calculated using AutoDock4.2). NHR, N-heptad repeat; CHR, C-heptad repeat.

quenching. The sensitivity of this experiment depended on the alignment of the fluorophore and metal complex, and C-peptides were designed with the fluorophore <18 Å from the metal. It was found that C-peptides designed for the receptors env5.1 and env6.0 were also quenched by env5.0, increasing the versatility of assay pairing.

Sequences of the peptides are indicated in *Table 3*. The wild-type (HXB2) sequence was used for all NHR peptides, to maintain receptor integrity for inhibitor detection, but C-peptides contained several helix-stabilizing modifications on the solvent-exposed face, based on studies demonstrating their effect on enhancing affinity.[8,19,20] Several C-peptide sequence variations were tested, with the sequences shown providing a good combination of high helicity and enhanced solubility.

NHR Trimer Formation

Metal binding to bipyridylated NHR peptides (env#) generally resulted in stabilization of the coiled coil, evidenced by an increase in helical content to 50% or higher in CD spectra and a 208 nm:222 nm peak intensity ratio of 1.0, which indicated α-helix bundle formation.[21] An exception was the peptide env4.0, which did not give a well-structured helical coiled coil upon metal binding and subsequently performed poorly in fluorescence experiments. An apparent helical content >100% was observed for the peptide env5.1 both in the absence and presence of Fe^{2+}. This was an indication of aggregation that was not ameliorated by metal binding, demonstrating a size limit of the self-assembly process in generating discreet trimers above a certain concentration. The CD results were confirmed by fluorescence studies (see below).

The receptor Fe(env6.0)$_3$ defined the region of gp41 at the base of the coiled coil, immediately adjacent to the fusion peptide proximal region that interacts with lipid membrane. A recent crystal structure of an extended segment of the gp41 ectodomain[22] revealed a loss of helical periodicity in the N-terminal region that is included in Fe(env6.0)$_3$ (*Fig. 1*). This did not appear to affect the formation of a well-formed trimer, although it may explain the lower helical content observed compared to other well-formed receptors. Fe(env6.0)$_3$ is the segment of the gp41 coiled coil to which T20 binds, including the residues $_{544}$LLSGIVQQQ$_{552}$ that are known to make important energetic interactions with T20.[16] Mutations within these residues are strongly associated with resistance to T20,[23–25] and a mutation of the T20 residue N656→L that binds to this segment abrogates fusion

Table 3. NHR (env#) and CHR (C*n*-e#) Assay Peptides[a]

Name	NHR peptides	% Helix[b]		$\theta_{208}/\theta_{222}$	
		$-Fe^{2+}$	$+Fe^{2+}$	$-Fe^{2+}$	$+Fe^{2+}$
env2.0	bpy-GQAVEAQQHLLQLTVWGIKQLQARILAVEKK-amide	24	59	1.6	1.0
env3.0	bpy-GQAVEAQQHLLQLTVWGIKQLQARILAVERYLKDQQKK-amide	70	72	1.0	1.0
env4.0	bpy-GQAVQAIEQQQNNLLRAIEAQQHLLQLTEKK-amide	26	34	1.6	1.3
env5.0	bpy-GQAVSGIVQQQNNLLRAIEAQQHLLQLTVWGIKQLQARILAVEKK-amide	54	69	1.0	1.0
env5.1	bpy-GQAVEAARQLLSGIVQQQNNLLRAIEAQQHLLQLTVWGIKQLQARILAVEKK-amide	120	134	0.9	1.0
env6.0	bpy-GQA**VE**Q**A**RQLLSGIVQQ**Q**NN**L**LRAIEA**Q**QHLLQL**T**EKK-amide	28	50	1.2	1.0
	CHR peptides	**% Helix[b]**		**% Change in complex[c]**	
C18-e2.0	Ac-MT**W**BE**W**DREIBN**Y**TSL**I**C-amide	17		+14	
C27-e3.0	Ac-KSLE**Q**BW**N**HTT**W**BE**W**DREIBN**Y**TSL**I**C-amide	12		+29	
C32-e5.0	Ac-TT**W**EA**W**DRAIAE**Y**AARIEAL**I**RA**A**QE**Q**QEK**N**C-amide	68		+13	
C39-e5.1	Ac-TT**W**EA**W**DRAIAE**Y**AARIEAL**I**RA**A**QE**Q**QEK**N**EAE**L**RE**L**C-amide	45		+23	
C28-e5.1	Ac-N**Y**AAL**I**EAL**I**RA**A**QE**Q**QEK**N**EAE**L**RE**L**C-amide	27		−9	
C21-e6.0	Ac-AL**I**RA**A**QE**Q**QEK**N**EAE**L**RE**L**C-amide	34		+19	
T20	638-**Y**TSL**I**HS**L**IEE**S**QN**Q**QEK**N**EQE**L**LEL**D**KWASLWNWF-673	n.d.		n.d.	

[a]# is a model number that refers to a particular construct of the NHR coiled coil; C-peptides are labeled by the number of residues *n* and a matching env#. C-peptides are fluorophore labeled at a C-terminal cysteine. Amino acids forming key interactions at *a* and *d* positions of the heptad repeat are indicated in bold. B is α-aminoisobutyric acid. T20 is included for reference, but is not an assay peptide.

[b]Determined by CD, using molar residue ellipticity of $-33{,}500$ degree·cm^{-2}·dmol^{-1} for 100% helix.

[c]Increase in helix content for the complex of C-peptide with cognate env# compared to the sum of component spectra.

NHR, N-heptad repeat; CHR C-heptad repeat.

completely.[26,27] This receptor target could be used to interrogate small molecule replacements of T20. It is also straightforward to modify the receptor for small molecule discovery to include common T20 resistance mutations.

CD Studies of Six-Helix Bundle Formation

A change in the CD signature for a mixture of receptor and C-peptide compared to the sum of individual spectra reflected complex formation. Example CD spectra are shown in *Figure 2* for the peptide pairs Fe(env5.1)$_3$/C39-e5.1, Fe(env5.1)$_3$/C28-e5.1, and Fe(env6.0)$_3$/C21-e6.0. An increase in helicity accompanied formation of the complex between cognate peptides Fe(env5.1)$_3$/C39-e5.1 and Fe(env6.0)$_3$/C21-e6.0, with the large negative molar residue ellipticity at both 222 and 208 nm indicative of six-helix bundle (6HB) formation.[21,28,29] Thus aggregation of Fe(env5.1)$_3$ did not preclude C-peptide binding. In *Figure 2B*, association of a truncated peptide C28-e5.1 with Fe(env5.1)$_3$ resulted in a distorted CD curve relative to that of the typical helix bundle. C28-e5.1 is missing the residues that bind in the HP, which is likely to lead to a combination of aggregation and an unstable six-helix structure. This effect has been observed in previous studies using T20 as the C-peptide.[17,30]

Fluorescence Studies of 6HB Formation

Dissociation constants (K_D) between peptide pairs were determined by direct titration of the Fe(env#)$_3$ receptor into a constant concentration of fluorescently labeled probe peptide.[13,15,29] Peptides were labeled with two different fluorescent probes, LY and FL. *Figure 4* demonstrates fluorescence quenching for several receptor/peptide pairs, and the fit to an equilibrium 1:1 binding model. The fluorescence quenching experiment with Fe(env5.1)$_3$ confirmed that it aggregated above 0.1 μM, with the concomitant loss in binding sites reflected in an increase in fluorescence at receptor concentrations exceeding 0.1 μM. The K_D's for all assay pairs are reported in *Table 4*. The assay pair Fe(env3.0)$_3$/C27-e3.0 ($K_D = 1.2 \pm 0.2$ μM) has been discussed elsewhere[14] and is not evaluated further here.

Inhibition constants were determined for unlabeled peptides, with the expectation that the observed K_I for a peptide inhibitor should equal the K_D of that peptide as a probe, barring any interference from

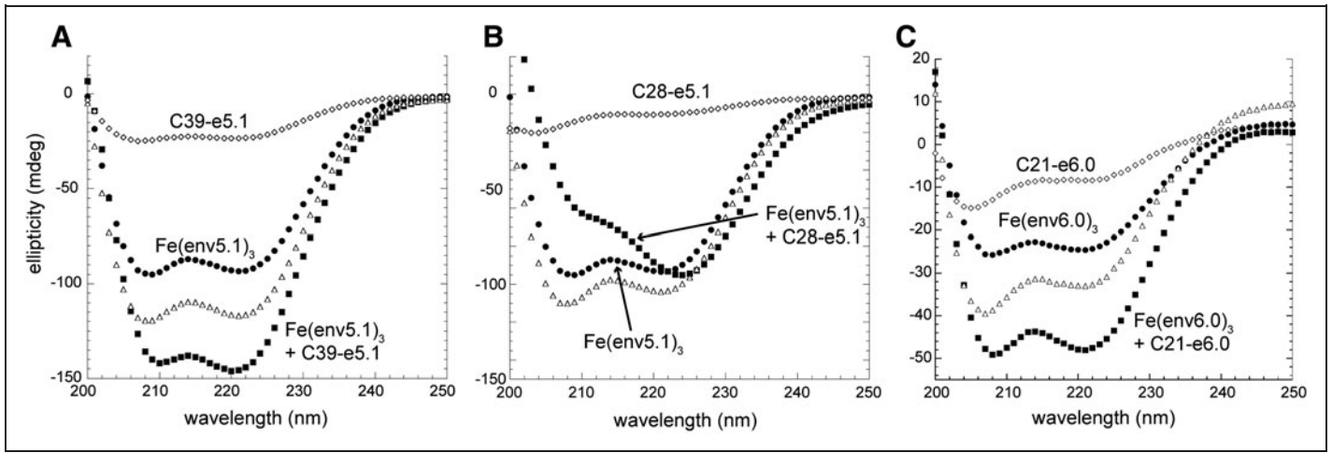

Fig. 2. Circular dichroism spectra for assay pairs using the long receptor Fe(env5.1)$_3$ **(A, B)** and the T20-binding site Fe(env6.0)$_3$ **(C)** The open triangles represents the sum of the C-peptide and Fe(env#)$_3$ spectra, the expected spectrum of the mixture if the peptides did not interact. All spectra were obtained at 20 μM peptide in a buffer at pH 7.

the fluorescent group. This was found to be the case with one exception (see below). K_I's are reported in *Table 5*. Fe(env5.1)$_3$ was not generally used as a receptor in inhibition experiments due to aggregation at the required concentrations. In the typical experiment, a probe and an inhibitor were premixed before adding a receptor, although in moderate affinity assays ($K_D \sim 1$ μM), rapid equilibrium was also achieved by adding the inhibitor to the premixed receptor and probe. K_D and K_I data enabled us to determine the energetic contribution of various subsites to 6HB formation, stability, and inhibition. K_D, or K_I in self-inhibition, is expected to reflect both the enthalpic contribution to binding energy from the length and characteristics of the helix–helix interface and the entropic penalty associated with C-peptide helical content changes (*Table 3*).[14] K_I in heterologous assays, on the other hand, could provide information about the contribution of a subsite in stabilizing the longer ectodomain.

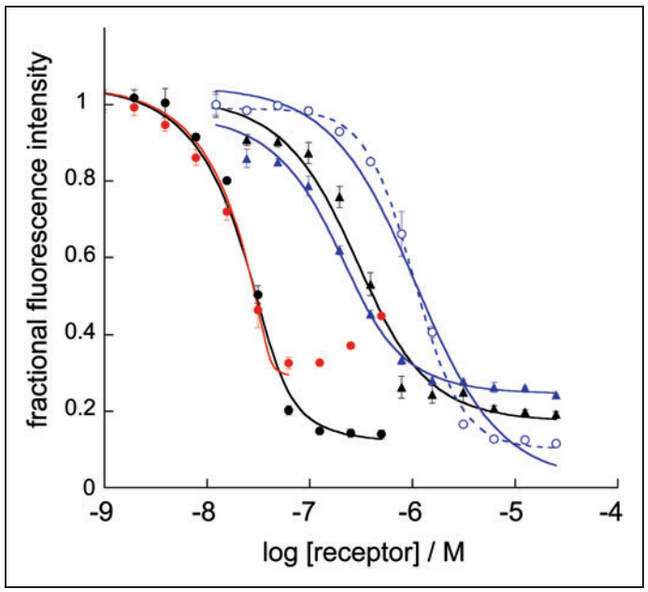

Fig. 3. Fluorescence-detected binding curves for env#/Cn-e# pairs depicted in *Figure 1*. Receptors used were env5.0 (black), env5.1 (red), or env6.0 (blue) and C-peptides used were C32-e5.0FL or C39-e5.1FL (closed circles), C28-e5.1LY (triangles) or C21-e6.0LY (open circles). Solid lines indicate fitting to a 1:1 binding model; the dashed line is a fit to IC_{50}. LY, lucifer yellow; FL, fluorescein. Color images available online at www.liebertpub.com/adt

The HP Plus About Five Residues Immediately Upstream was the Only Significant Hotspot Mediating the Helix–Helix Interaction

C32-e5.0 had 50-fold increased affinity over C28-e5.1 for Fe(env5.0)$_3$, highlighting the importance of the HP-binding region, in agreement with previous binding and mutagenesis studies.[31–33] C21-e6.0, directed to the region of the NHR that readily mutates upon exposure of the intact virus to T20, had 10-fold reduced affinity compared to C28-e5.1, indicating that important interactions with the NHR involved the segment $_{637}$NYTSLI$_{642}$ (wild-type sequence, residues in bold interact in the NHR groove). Truncated T20 variants missing this segment demonstrated a dramatic loss of antiviral potency.[34] These residues were also essential for the 0.8 μM affinity of the HP-binding peptide C18-e2.0 (unpublished observation and reference[35]), although they are not considered to be part of the pocket-binding domain.

Inhibition data in heterologous assays confirmed the expanded HP interaction with C18-e2.0 as the most significant hotspot mediating 6HB formation. Thus, C18-e2.0 was able to inhibit the much longer Fe(env5.0)$_3$–C32-e5.0FL interface at about the same K_I as for self-inhibition, while peptides corresponding to other segments (C28-e5.1,

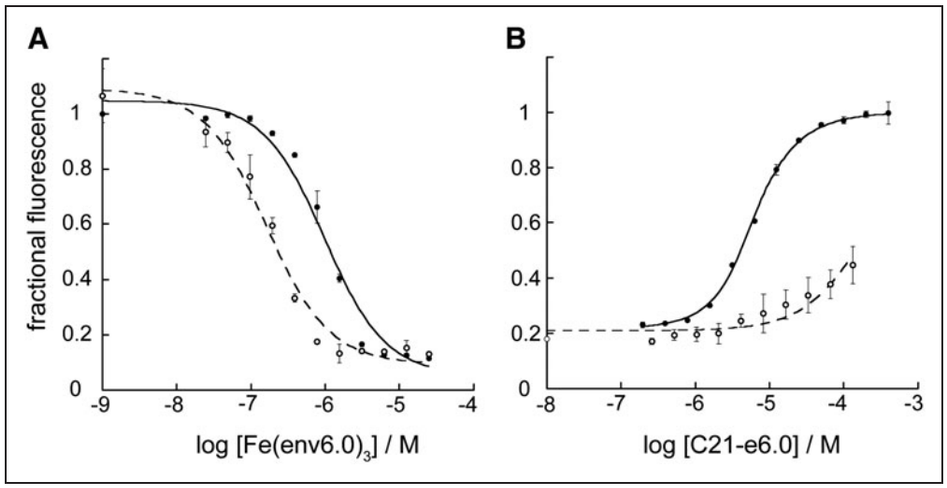

Fig. 4. Dissociation and inhibition constant determination for the assay pair $Fe(env6.0)_3$/C21-e6.0. **(A)** Binding of receptor $Fe(env6.0)_3$ to 0.2 μM C21-e6.0LY (solid circles) and 15 nM C21-e6.0FL (open circles). **(B)** Inhibition curves using 3 μM $Fe(env6.0)_3$ and 0.2 μM C21-e6.0LY (solid circles) or 0.75 μM $Fe(env6.0)_3$ and 15 nM C21-e6.0FL (open circles). The inhibitor C21-e6.0 was mixed with a probe peptide before adding a receptor.

C21-e6.0) had significantly reduced ability to compete with C32-e5.0FL compared to inhibition of self.

Interactions Between NHR and CHR at the Base of the Coiled Coil were Energetically Significant, but Could not Inhibit 6HB Formation

The peptide pair $Fe(env6.0)_3$ and C21-e6.0 representing the base of the 6HB formed a complex with a 1 μM K_D/K_I, a reasonably strong association, involving both hydrophobic and polar interactions (*Fig. 1*). The NHR segment $_{540}$QARQLL$_{545}$ provided for a two-fold increase in binding potency with peptides C21-e6.0LY or C28-e5.1LY, as could be seen by comparing K_D's obtained with $Fe(env6.0)_3$ or $Fe(env5.1)_3$ with those obtained with $Fe(env5.0)_3$. The viral fusion-inactivating N656L mutation on the CHR[26] reduced affinity of C21-e6.0 by a factor of 7 for receptor $Fe(env6.0)_3$, 7.6 for receptor $Fe(env5.1)_3$ (data not shown), and 25 for receptor $Fe(env5.0)_3$. Differences in the effect of the mutation appeared to be due to compensatory interactions of C21-e6.0 with $_{540}$QARQLL$_{545}$.

The reduction of potency of C21-e6.0 in heterologous assays was particularly striking, since it was unable to displace either C32-e5.0FL or C28-e5.1FL/LY from $Fe(env5.0)_3$ at concentrations up to 200 μM. It displaced C28-e5.1FL/LY from $Fe(env6.0)_3$ with six-fold reduced K_I compared to inhibition of self, and was unable to displace C21-e6.0FL. There is an overwhelming evidence from structural and mutagenesis studies that the NHR–CHR interaction spanned by $Fe(env6.0)_3$–C21-e6.0 forms part of the 6HB core, and plays a critical role in gp41 function.[22,27] Thus, while there is clear evidence for NHR–CHR stabilizing interactions in this region, our data and other studies[36] suggest they do not appear to play a central role in disrupting or preventing 6HB formation.

Table 4. Dissociation Constants in μM of Receptor–Probe Pairs Used in Fluorescence Assays[a]

Probe	$Fe(env2.0)_3^{2+}$	$Fe(env5.0)_3^{2+}$	$Fe(env5.1)_3^{2+}$	$Fe(env6.0)_3^{2+}$
C18-e2.0LY	0.8 ± 0.2			
C18-e2.0FL	0.6 ± 0.2			
C32-e5.0FL		0.004 ± 0.002		
C39-e5.1FL		0.003 ± 0.002	~0.013	
C28-e5.1LY		0.23 ± 0.02	0.09 ± 0.2	0.10 ± 0.02
C28-e5.1FL		0.18 ± 0.05	0.02 ± 0.004	0.03 ± 0.01
C21-e6.0LY		2.2 ± 0.33	1.1 ± 0.1	1.1 ± 0.2
C21-e6.0FL		~2.5[b]	0.09 ± 0.02	0.33 ± 0.08

[a]Receptor peptides are named env followed by a version number, probe peptides are labeled Cn followed by a version number. Experiments were repeated in quadruplicate and on at least two different days for each assay pair. The standard deviation is shown. Shaded areas correspond to noncompatible pairs.

[b]Estimated from the IC_{50} (see text).

n, number of residues.

The Base of the Coiled Coil Showed Conformational Variability and Flexibility

Effects, including nonspecific hydrophobic interactions and deviations from 1:1 binding in constructs containing residues at the base of the coiled coil, were suggestive of conformational flexibility in this region. The segment $_{540}$QARQLL$_{545}$ was implicated in nonspecific binding of the hydrophobic C-terminal FL group, which interfered in assays with $Fe(env5.1)_3$ or $Fe(env6.0)_3$, resulting in an observed K_D of FL-labeled peptides three-fold lower than the K_D for the corresponding LY-labeled peptides (*Fig. 4A*; *Table 4*) or the K_I of unlabeled peptides (*Table 5*). No association with free FL was observed. It was further found that unlabeled C21-e6.0 could not displace C21-e6.0FL from $Fe(env6.0)_3$, while readily displacing C21-e6.0LY (*Fig. 4B*), or either the probe peptide from the receptor $Fe(env5.0)_3$. Interestingly, FL-labeling resulted in a K_D closer to the 100 nM K_I observed for T20 binding to $Fe(env6.0)_3$. T20 showed mid-nM inhibition in all

Table 5. Inhibition Constants in μM for C-Peptide and Small Molecule Inhibitors Using Several Assay Pairs[a]

	$Fe(env2.0)_3$ C18-e2.0FL/LY	$Fe(env5.0)_3$ C32-e5.0FL	$Fe(env5.0)_3$ C28-e5.1FL/LY	$Fe(env5.0)_3$ C21-e6.0FL/LY	$Fe(env6.0)_3$ C21-e6.0FL/LY	
Inhibitor					LY	FL
C18-e2.0	0.8 (0.2)	1.1 (0.3)				
C28-e5.1		1.4 (0.2)	0.3 (0.1)	0.2 (0.1)	0.45 (0.15)	
C21-e6.0		*> 500*	*> 150*	4.9 (0.5)	0.8 (0.1)	~60
C21-e6.0 N656L		*> 500*	> 150	126 (11)	5.6 (1)	~150
T20	1.4 (0.3)	0.3 (0.1)	0.2 (0.04)	0.05 (0.01)	0.1 (0.03)	
3a (MW 251)	3 (1)	8.5 (1.6)	69 (14)	139 (24)	184 (24)	
14c (MW 357)	2.3 (0.3)	22 (1.5)	112 (16)	nsb, *IC_{50} = 63*[b]	nsb, *IC_{50} = 281*[b]	
14g (MW 487)	1.1 (0.2)	1.8 (0.5)	1.7 (0.3)	4.1 (0.6)	nsb, *IC_{50} = 55*[b]	

[a]Inhibition constants obtained by competitive inhibition using the indicated metal-chelated NHR peptide Env# and fluorescently labeled CHR-peptide probe. In brackets is the standard deviation. Except where indicated, both probes gave the same K_I. Hatched cells indicate no or poor overlap of the peptide inhibitor with an assay probe.

[b]Nonspecific binding, IC_{50} in italics, sharp rise (Hill coefficient > 2.5).

AU5

assays except $Fe(env2.0)_3$–C18FL, which was to be expected, since T20 does not contain HP-binding residues. The hydrophobic tail of T20 binds to the fusion-peptide proximal region, which is not included in env6.0. Therefore some nonspecific hydrophobic effect was occurring with T20 as well.

The nonspecific binding resulted in deviations from normal 1:1 binding with C21-e6.0FL and to a lesser extent C21-e6.0LY. Binding curves displayed sharp transitions with a Hill coefficient > 1.5 (*e.g.*, *Fig. 4A*). The fluorescent label appeared to be a principle factor in inducing the effect, since unambiguous 1:1 binding was observed in the inhibition data for C21-e6.0 (*Fig. 4B*). The effect was observed only for the 21-residue peptide, where nonspecific interactions could likely contribute a significant proportion of the affinity. Some type of distortion is necessary to explain the fluorophore interaction, since it was designed to point away from the NHR–CHR interface in a purported six-helix structure. The observed cooperative binding transition may be associated with conformational variation from the expected six-helix structure. A recent crystal structure of full length ectodomain, including the membrane proximal external region (MPER), indicated that splaying and loss of the NHR helical structure occurred in this region.[22] It is possible that FL could partially mimic the MPER in inducing a structural change.

High-Affinity Small Molecule Binding was Specific to the HP and Suggested a Dependence of Potency on Off-Rate

Assay performance was evaluated for potency and specificity with several confirmed low to sub-μM HP-binding inhibitors.[18] Three of these, **6a**, **14c**, and **14g** are listed in *Table 5*, together with K_I's determined in all assays. They were selected because they have similar affinities in the HP-binding assay $Fe(env2.0)_3$/C18-e2.0, but differ in their ability to impede fusion.[18] IC_{50}'s for fusion inhibition were 5, 8, and 0.8 μM, respectively, for **6a**, **14c**, and **14g**. **14g** (plus some similar unpublished derivatives) is the only verified sub-μM fusion inhibitor in this scaffold class and is also the only small molecule tested in our laboratory to efficiently block the extended $Fe(env5.0)_3$–C32-e5.0FL helical interaction. To investigate whether this property could contribute to its improved biological activity, the assay suite was used to investigate the mechanism.

6a and **14c** were weak or nonspecific inhibitors in all assays other than the HP-binding assay $Fe(env2.0)_3$–C18-e2.0. The inhibition curves for **14g** in *Figure 5A* demonstrated low μM inhibition of the interactions $Fe(env2.0)_3$–C18-e2.0, and $Fe(env5.0)_3$–C32-e5.0. Minimal inhibition in the $Fe(env6.0)_3$–C28-e5.1 assay implied that the molecule was located specifically within the confines of the HP.[15] Additional nonspecific inhibition occurred at the base of the coiled coil, as evidenced by a sharp rise in signal in assays with $Fe(env6.0)_3$ and C21-e6.0FL/LY at high inhibitor concentrations. However, unexpectedly, **14g** inhibited C28-e5.1 and C21-e6.0 binding to $Fe(env5.0)_3$, with an apparent 1:1 binding mechanism, contrary to the results obtained with $Fe(env6.0)_3$. Further experimentation revealed that **14g** did not inhibit C28-e5.1 or C21-e6.0 binding to $Fe(env5.1)_3$ (except nonspecifically at high concentrations). Rather, it increased the amount of bound C-peptide as evidenced by a reduction in baseline fluorescence upon addition of up to 25 μM **14g** (*Fig. 5B*). The increased availability of binding sites for the probe peptide is presumed due to reduction of aggregation of the receptor when **14g** occluded the HP. At concentrations above 25 μM, the familiar nonspecific binding of **14g** to the base of the 6HB occurred. For comparison, 1:1 binding of C21-e6.0 due to competitive inhibition of $Fe(env5.1)_3$–C21-e6.0LY is shown in *Figure 5B*.

F5

The apparent inhibition by **14g** of C28-e5.1LY and C21-e6.0LY binding to $Fe(env5.0)_3$ appeared to be spurious in that it did not represent competitive inhibition of the NHR–CHR interaction. The only difference between this receptor and $Fe(env5.1)_3$ is the presence in the latter of the additional segment $_{540}$QARQLL$_{545}$, which has been associated with nonspecific binding of both fluorescently labeled C-peptide and **14g**. Indeed, nonspecific binding of **14g** to $Fe(env5.0)_3$ was not observed. It is likely that $Fe(env5.0)_3$ is not an ideal assay partner for C21-e6.0FL/LY and C28-e5.1FL/LY, despite quenching

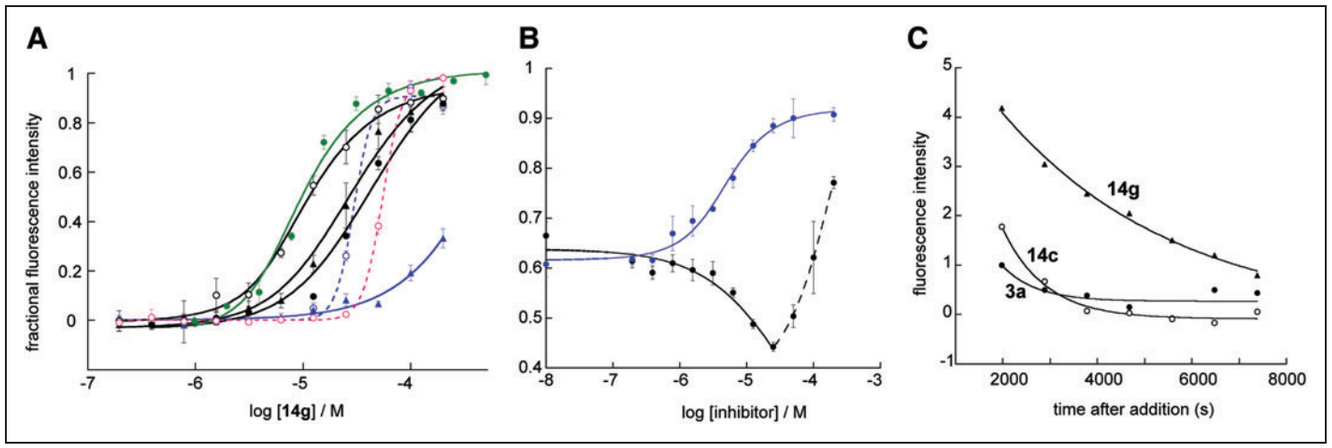

Fig. 5. **(A)** Inhibition curves for **14g** in various assays. Receptors used were Fe(env2.0)$_3$ (green), Fe(env5.0)$_3$ (black), or Fe(env6.0)$_3$ (blue, pink). C-peptide probes were C18-e2.0FL (green circles), C32-e5.0FL (black circles), C28-e5.1LY (triangles), C21-e6.0LY/FL (open circles). Solid lines are a fit to a 1:1 binding model, providing the K_I. Dashed lines are a fit to the IC_{50} and are colored blue and pink for probes C21-e6.0LY and C21-e6.0FL, respectively. The y-axis is scaled for a minimum fluorescence of 0. **(B)** Inhibition of the interaction of 1.8 μM Fe(env5.1)$_3$ and 0.2 μM C21-e6.0LY by C21-e6.0 (blue) and **14g** (black). **(C)** Fluorescence intensity as a function of time after addition of C32-e5.0FL to a mixture of Fe(env5.0)$_3$ (75 nM) and **3a** (6.25 μM, closed circles), **14c** (6.25 μM, open circles), and **14g** (3.13 μM, closed triangles). Results from dimethyl sulfoxide only controls have been subtracted from the data. Early data points (< 2,000 s) are omitted due to artifacts of physical mixing. Color images available online at www.liebertpub.com/adt

the fluorescence of these peptides upon binding. It appeared that the C-terminal heptad overhang of the probe peptides, and the metal binding group of the receptor (*Fig. 1*) generated a non-natural site for **14g** binding.

Having ruled out multiple-site binding for **14g** as a mechanism for its increased potency in the high-affinity assay Fe(env5.0)$_3$–C32-e5.0FL and in fusion inhibition, off-rate was examined as a possible contributor to potency. Off-rate can be slowed by a protein conformational change associated with ligand binding.[37] Order of addition assays were used to obtain a rough estimate of the on and off-rates for C32-e5.0 with the receptor Fe(env5.0)$_3$, yielding $k_{on} = 10^5\ M^{-1}\ s^{-1}$ and $k_{off} = 0.0004\ s^{-1}$, which is within an order of magnitude of off-rates determined for a slightly longer peptide C37 in situ[38] (*Supplementary Fig. S1*; Supplementary Data are available online at www.liebertpub.com/adt). The slow kinetics permitted us to evaluate the effect of a small molecule ligand bound to Fe(env5.0)$_3$ by premixing the receptor with a low concentration of the ligand, and observing the time to equilibrium after adding C32-e5.0FL. This experiment is shown in *Figure 5C* for the ligands **3a**, **14c**, and **14g**, and suggested three to five times slower off-rate for **14g** than for **3a** and **14c** (see also *Supplementary Fig. S1*). Thus, the increased potency of **14g** over earlier derivatives **3a** and **14c** could be attributed to differences in binding kinetics.

CONCLUSIONS

This study demonstrated a suite of assays for probing binding and segmental activity of the coiled coil domain of HIV-1 gp41. The assays encompass HP or T20 subsite detection, as well as full-length 6HB coverage. Dissociation and inhibition constants for peptides and small molecules accurately reflected both affinity and specificity provided the CHR probe peptide had a complete cognate-binding site on the Fe(env#)$_3$ receptor. The assay Fe(env6.0)$_3$/C21-e6.0LY, simulating the T20-binding site where resistance mutations are common, is the newest addition to our repertoire for examining gp41. The 1 μM K_D indicates that it can be used to detect inhibitors in the low μM to mM range that have a unique binding site apart from the HP. Experiments here demonstrate that use of the probe peptide in its LY-labeled form will be preferential over FL-labeling.

Importantly, many of the biophysical results that were obtained matched very well with observed biological data. The assays revealed that the HP was the sole hotspot mediating the NHR–CHR interaction, conferring significant stability to the 6HB. The first five residues of T20, which are critical for antiviral activity, were also necessary for high-affinity binding to the coiled coil. Peptides containing a known inactivating mutation N656L displayed a dramatic loss of potency. Evidence for a break in the rigid helical structure toward the base of the coiled coil was obtained, both from the inability of a C-peptide from this region to disrupt 6HB formation and from indication of conformational flexibility upon probe binding. The assay representing the 6HB segment at the base of the coiled coil showed unique features compared to the other assays, including interference of the FL group in binding, resulting in a cooperative binding transition, inability of the unlabeled peptide to compete with its FL-labeled counterpart, and nonspecific binding of hydrophobic compounds. The overall agreement between known biological properties and observed binding properties of the C-peptides confirmed the

accuracy of the metallopeptide receptor models in representing the intact gp41 NHR trimer.

Evaluation of a sub-μM small molecule fusion inhibitor revealed that it was able to effectively inhibit the high-affinity interaction between a 40-residue NHR construct and a 32-residue CHR peptide. Small molecules that were not able to inhibit this interaction in the low to sub-μM range were found to have ≥10-fold weaker activity against cell–cell fusion, even if they had similar ability to disrupt an 18-residue CHR peptide binding in the HP. This property is demonstrated here with just three inhibitors, but recent results (unpublished) have indicated that it applies more broadly and may be a unique identifying property of effective low molecular weight fusion inhibitors. The mechanism of extended NHR–CHR inhibition appears to be associated with lower off-rate of the small molecule ligand, with binding specificity restricted to the HP. The assay suite could be used to aid in the discovery of alternative ligands, which bind adjacent to the pocket and, which could be tethered to HP-binding inhibitors, leading to a significant increase in potency.

ACKNOWLEDGMENTS

This work was supported by NIH grants NS066469 and GM087998. I thank Dr. Richard Shafer, UCSF, for use of the CD machine and Dr. G. Zhou for providing the low molecular weight compounds tested in the assays. Molecular graphics images were produced using Chimera, developed by the Resource for Biocomputing, Visualization, and Informatics at the University of California, San Francisco, with support from the NIH (National Center for Research Resources grant 2P41RR001081, NIGMS 9P41GM103311).

DISCLOSURE STATEMENT

No competing financial interests exist.

REFERENCES

1. Teissier E, Penin F, Pecheur EI: Targeting cell entry of enveloped viruses as an antiviral strategy. *Molecules* 2011;16:221–250.
2. Naider F, Anglister J: Peptides in the treatment of AIDS. *Curr Opin Struct Biol* 2009;19:473–482.
3. Jacobs A, Garg H, Viard M, Raviv Y, Puri A, Blumenthal R: HIV-1 envelope glycoprotein-mediated fusion and pathogenesis: implications for therapy and vaccine development. *Vaccine* 2008;26:3026–3035.
4. Groot F, Welsch S, Sattentau QJ: Efficient HIV-1 transmission from macrophages to T cells across transient virological synapses. *Blood* 2008;111: 4660–4663.
5. Eckert DM, Kim PS: Mechanisms of viral membrane fusion and its inhibition. *Annual Rev Biochem* 2001;70:777–810.
6. Wild C, Oas T, McDanal C, Bolognesi D, Matthews T: A synthetic peptide inhibitor of human immunodeficiency virus replication: correlation between solution structure and viral inhibition. *Proc Natl Acad Sci U S A* 1992;89: 10537–10541.
7. Jiang S, Lin K, Strick N, Neurath AR: HIV-1 inhibition by a peptide. *Nature* 1993;365:113.
8. Dwyer JJ, Wilson KL, Davison DK, Freel SA, Seedorff JE, Wring SA, Tvermoes NA, Matthews TJ, Greenberg ML, Delmedico MK: Design of helical, oligomeric HIV-1 fusion inhibitor peptides with potent activity against enfuvirtide-resistant virus. *Proc Natl Acad Sci U S A* 2007;104:12772–12777.
9. Manfredi R, Sabbatani S: A novel antiretroviral class (fusion inhibitors) in the management of HIV infection. Present features and future perspectives of enfuvirtide (T-20). *Curr Med Chem* 2006;13:2369–2384.
10. Gochin M, Zhou G: Amphipathic properties of HIV-1 gp41 fusion inhibitors. *Curr Topics Med Chem* 2011;11:3022–3032.
11. Cai L, Jiang S: Development of peptide and small-molecule HIV-1 fusion inhibitors that target gp41. *Chem Med Chem* 2010;5:1813–1824.
12. Hajduk PJ: SAR by NMR: putting the pieces together. *Mol Interv* 2006;6:266–272.
13. Cai L, Gochin M: A novel fluorescence intensity screening assay identifies new low molecular weight inhibitors of the gp41 coiled coil domain of HIV-1. *Antimicrob Agents Chemother* 2007;51:2388–2395.
14. Gochin M, Cai L: The role of amphiphilicity and negative charge in glycoprotein 41 interactions in the hydrophobic pocket. *J Med Chem* 2009;52:4338–4344.
15. Cai L, Balogh E, Gochin M: Stable extended human immunodeficiency virus type 1 gp41 coiled coil as an effective target in an assay for high-affinity fusion inhibitors. *Antimicrob Agents Chemother* 2009;53:2444–2449.
16. McGillick BE, Balius TE, Mukherjee S, Rizzo RC: Origins of resistance to the HIVgp41 viral entry inhibitor T20. *Biochemistry* 2010;49:3575–3592.
17. Liu S, Jing W, Cheung B, Lu H, Sun J, Yan X, Niu J, Farmar J, Wu S, Jiang S: HIV gp41 C-terminal heptad repeat contains multifunctional domains. Relation to mechanisms of action of anti-HIV peptides. *J Biol Chem* 2007;282:9612–9620.
18. Zhou G, Wu D, Snyder B, Ptak RG, Kaur H, Gochin M: Development of indole compounds as small molecule inhibitors of HIV-1 gp41. *J Med Chem* 2011;54: 7220–7231.
19. Oishi S, Ito S, Nishikawa H, Watanabe K, Tanaka M, Ohno H, Izumi K, Sakagami Y, Kodama E, Matsuoka M, Fujii N: Design of a novel HIV-1 fusion inhibitor that displays a minimal interface for binding affinity. *J Med Chem* 2008;51:388–391.
20. Otaka A, Nakamura M, Daisuke N, Kodama E, Uchiyama S, Nakamura H, Kobayashi Y, Matsuoka M, Fujii N: Remodelling of gp41-C34 peptide leads to highly effective inhibitors of the fusion of HIV-1 with target cells. *Angew Chem Int Ed* 2002;41:2938–2939.
21. Cohen C, Parry DA: Alpha-helical coiled coils and bundles: how to design an alpha-helical protein. *Proteins* 1990;7:1–15.
22. Buzon V, Natrajan G, Schibli D, Campelo F, Kozlov MM, Weissenhorn W: Crystal structure of HIV-1 gp41 including both fusion peptide and membrane proximal external regions. *PLoS Pathog* 2010;6:e1000880.
23. Greenberg ML, Cammack N: Resistance to enfuvirtide, the first HIV fusion inhibitor. *J Antimicrob Chemother* 2004;54:333–340.
24. Armand-Ugon M, Gutierrez A, Clotet B, Este JA: HIV-1 resistance to the gp41-dependent fusion inhibitor C-34. *Antiviral Res* 2003;59:137–142.
25. Rimsky LT, Shugars DC, Matthews TJ: Determinants of human immunodeficiency virus type 1 resistance to gp41-derived inhibitory peptides. *J Virol* 1998;72:986–993.
26. Cao J, Bergeron L, Helseth E, Thali M, Repke H, Sodroski J: Effects of amino acid changes in the extracellular domain of the human immunodeficiency virus type 1 gp41 envelope glycoprotein. *J Virol* 1993;67:2747–2755.
27. Chan DC, Fass D, Berger JM, Kim PS: Core structure of gp41 from the HIV envelope glycoprotein. *Cell* 1997;89:263–273.
28. Sackett K, Wexler-Cohen Y, Shai Y: Characterization of the HIV N-terminal fusion peptide-containing region in context of key gp41 fusion conformations. *J Biol Chem* 2006;281:21755–21762.
29. Gochin M, Guy RK, Case MA: A metallopeptide assembly of the HIV-1 gp41 coiled coil is an ideal receptor in fluorescence detection of ligand binding. *Angew Chem Int Ed* 2003;42:5325–5328.
30. Wild C, Greenwell T, Shugars D, Rimsky-Clarke L, Matthews T: The inhibitory activity of an HIV type 1 peptide correlates with its ability to interact with a leucine zipper structure. *AIDS Res Hum Retroviruses* 1995;11:323–325.
31. Mo H, Konstantinidis AK, Stewart K, Dekhtyar T, Ng T, Swift K, Matayoshi E, Kati W, Kohlbrenner W, Molla A: Conserved residues in the coiled-coil pocket of human immunodeficiency virus type 1 gp41 are essential for viral replication and interhelical interaction. *Virology* 2004;329:319–327.

32. Chan DC, Chutkowski CT, Kim PS: Evidence that a prominent cavity in the coiled coil of HIV type 1 gp41 is an attractive drug target. *Proc Natl Acad Sci U S A* 1998;95:15613–15617.
33. He Y, Liu S, Jing W, Lu H, Cai D, Chin DJ, Debnath AK, Kirchhoff F, Jiang S: Conserved residue Lys574 in the cavity of HIV-1 Gp41 coiled-coil domain is critical for six-helix bundle stability and virus entry. *J Biol Chem* 2007;282: 25631–25639.
34. Wild CT, Shugars DC, Greenwell TK, McDanal CB, Matthews TJ: Peptides corresponding to a predictive alpha-helical domain of human immunodeficiency virus type 1 gp41 are potent inhibitors of virus infection. *Proc Natl Acad Sci U S A* 1994;91:9770–9774.
35. Cole JL, Garsky VM: Thermodynamics of peptide inhibitor binding to HIV-1 gp41. *Biochemistry* 2001;40:5633–5641.
36. Liu S, Lu H, Niu J, Xu Y, Wu S, Jiang S: Different from the HIV fusion inhibitor C34, the anti-HIV drug Fuzeon (T-20) inhibits HIV-1 entry by targeting multiple sites in gp41 and gp120. *J Biol Chem* 2005;280: 11259–11273.
37. Cai L, Zhou HX: Theory and simulation on the kinetics of protein-ligand binding coupled to conformational change. *J Chem Phys* 2011;134:105101.
38. Kahle KM, Steger HK, Root MJ: Asymmetric deactivation of HIV-1 gp41 following fusion inhibitor binding. *PLoS Pathog* 2009;5:e1000674.
39. Caffrey M: Model for the structure of the HIV-1 gp41 ectodomain: insight into the intermolecular interactions of the gp41 loop. *Biochim Biophys Acta* 2001; 1536:116–122.

Address correspondence to:
Miriam Gochin, Ph.D.
Touro University California
1310 Club Drive
Mare Island
Vallejo 94592, CA

E-mail: miriam.gochin@tu.edu

AU1 Please review all authors' surnames for accurate indexing citations.
AU2 Please expand FDA, HPLC, TFA, and PDB.
AU3 Figure 3 not cited in text. Please check.
AU4 Please define n.d. in Table 3.
AU5 Significance of shaded areas not given in table 5 footnote. Please check.
AU6 Part figures A–C mentioned in artwork, but not provided in figure S1 legend. Please check.

SUPPLEMENTARY DATA

NUMERICAL ESTIMATE OF k_{on} AND k_{off}

The time course of fluorescence of a ternary system containing receptor R, probe P, and inhibitor I was evaluated using equilibrium and mass balance equations for standard 1:1 binding

$$R + P \underset{k_{1off}}{\overset{k_{1on}}{\rightleftharpoons}} RP \qquad K_D = [R]^*[P]/[RP] = k_{1off}/k_{1on}$$

$$+$$

$$I \qquad K_I = [R]^*[I]/[RI] = k_{2off}/k_{2on}$$

$$k_{2off} \rightleftharpoons k_{2on} \qquad R_t = [R] + [RI] + [RP]$$

$$P_t = [P] + [RP]$$

$$RI \qquad I_t = [I] + [RI]$$

with the observed fluorescence at time t defined as the weighted average of the signals of free and bound probe,

$$F_{obs}(t) = F_{min}[RP]/P_t + F_{max}[P]/P_t$$

F_{max} and F_{min} are the fluorescence intensities observed for probe P_t free and in the complex RP, respectively, and concentrations in square brackets are implicitly a function of t. The concentration of each species at time t is governed by kinetic equations:

$$d[R]/dt = -k_{1on}[R][P] - k_{2on}[R][I] + k_{1off}[RP] + k_{2off}[RI]$$

$$d/[P]/dt = -k_{1on}[R][P] + k_{1off}[RP]$$

$$d[RP]/dt = k_{1on}[R][P] - k_{1off}[RP]$$

$$d[I]/dt = -k_{2on}[R][I] + k_{2off}[RI]$$

$$d[RI]/dt = k_{2on}[R][I] - k_{2off}[RI]$$

The differential equations were programmed into Mathcad (Mathsoft). Initial conditions and total concentrations of components were set according to the experimental setup (see caption to *Supplementary Fig. S1*). Dissociation and inhibition constants K_D and K_I were taken from Tables 4 and 5. The solution to the differential equations was obtained using the Rkadapt function, returning species concentrations from which $F_{obs}(t)$ was calculated. The kinetic parameters k_{1off} and k_{2off} were varied to obtain a best fit to the data shown in *Supplementary Figure S1*.

The slow on-rate for **14c** and **14g** may be due to slow mixing of the DMSO, and may be an artifact of the assays given that up to 30 min was required to reach equilibrium of DMSO-only solutions after manual mixing in the 384-well plates. Relative rates between different compounds dissolved in DMSO can be compared, but absolute rates are not definitive. AU6

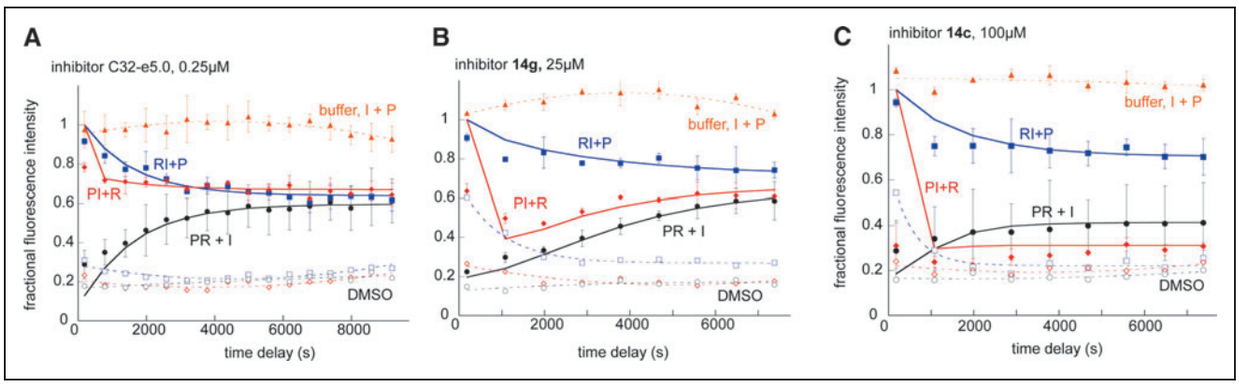

Supplementary Fig. S1. Order of addition assays with $Fe(env5.0)_3$–C32-e5.0FL. P, R, and I are C32-e5.0FL, $Fe(env5.0)_3$, and indicated inhibitor, respectively. **14c** and **14g** were added as dimethyl sulfoxide (DMSO) solutions. Fluorescence was measured over time as a function of the order in which components were mixed in the assay. The symbol after the plus sign indicates the component that was added last. Experiments were conducted in a 384-well plate after manual mixing and the fluorescence followed over 2 h. Also shown are responses when the inhibitor was omitted from the DMSO solution. Data were fit numerically to standard 1:1 binding and mass balance equations using Mathcad (Mathsoft). The kinetic parameters obtained for the curves shown in the figure are as follows:

Inhibitor	K_D (μM)	K_I (μM)	k_{on} (M^{-1} s^{-1})	k_{off} (s^{-1})
C32-e5.0	0.004	0.004	10^5	0.0004
14g	0.004	1.8	33 (15)	0.0001(1)
14c	0.004	23	35 (15)	0.0008(2)